scientific reports

OPEN

Graphene-based LSPR sensors enable polarization-independent detection of CEA antigens

Yousef Rafighirani, Hamid Bahador✉ & Javad Javidan

This study presents a biosensor based on cleaved graphene, compared with a graphene-gold nanoparticle structure, for detecting carcinoembryonic antigen (CEA), leveraging graphene's tunable resonance frequency and the structure's polarization-independent performance. This sensor consists of three layers: a gold substrate with a conductivity of 4.7×10^7, a silicon dioxide (SiO_2) dielectric layer with a permeability of 3.9, and a graphene layer with strategic cuts to increase absorption. The performance of the proposed structure has been measured by measuring its absorption around the 8.9 terahertz frequency band, which has reached absorption values above 99.4–99.9% for the first structure and absorption above 99.6–100% for the second structure, which includes graphene plus gold nanoparticles, respectively. These high absorption rates make the sensor an excellent candidate for biosensing applications, especially for the detection of CEA in clinical samples. By testing the sensor with analytes containing CEA in concentrations of 1, 2, 3, 4, and 5 ng/ml, the refractive index values were 1.3337, 1.33374, 1.3448, and 1.3485, respectively. When the analyte layer is placed on the three-band absorber structure, the peak shift is absorbed and allows the detection of the desired analyte. The second proposed structure showed significant sensitivity and achieved 4.3 THz / RIU at 1.3411 refractive index and 8.8483 THz frequency, LOD = 0.001 and FOM = 26. This high sensitivity is especially useful for detecting low concentrations of analyte. Such a sensor has a high potential to increase the detection of biomarkers. These findings highlight the potential of the sensor for CEA detection with high sensitivity.

Keywords Biosensor, Graphene heterogeneous structure, Terahertz, Metamaterial, Reflectivity index

In recent decades, nanomaterial sensors have been widely considered as advanced tools for detecting biological molecules and medical biomarkers. These sensors are characterized by unique nanomaterial features, including high surface-to-volume ratios, unparalleled electronic and optical properties, and surface chemical modification capabilities, have been able to make significant advances in biological and medical sciences[1]. One of these important biomarkers is the carcinoembryonic antigen (CEA), mainly used in diagnosing and monitoring cancers[2].

CEA is a glycoprotein naturally expressed in the early stages of fetal development, but levels are typically very low in adults. Increased levels of CEA in the blood are usually associated with the occurrence and progression of some cancers, including colorectal cancer, lung cancer, pancreatic cancer, and breast and ovarian cancer[3]. For this reason, this molecule is known as a valuable biomarker (biomarker) for screening, early detection, and monitoring of cancer progression[4]. Nanomaterial-based sensors, such as carbon nanotubes, quantum dots, graphene, and metal nanoparticles, provide the ability to detect CEA with high precision. These sensors operate in a variety of ways, such as optical spectroscopy, voltameters, and modified electrodes. For example, gold nanoparticles, due to their strong plasmonic properties and high bio-connectivity, have been used in the manufacture of electrochemical sensors to identify CEA[5]. Also, the use of graphene due to its high electrical conductivity and its two-dimensional structure allows the detection of very low values of CEA[6,7].

The benefits of using these sensors include high sensitivity and accuracy, short response time, and the possibility of simultaneous identification of several biological molecules. These features not only help improve the diagnosis of cancer but also play a role in the development of new therapies[8]. Due to the strong association of CEA with different types of cancers, the development of new sensors and the optimization of existing technologies are essential for accurate and rapid measurement of this antigen. Recent research has shown that combining nanomaterials with proprietary biomolecules such as antibodies or aptamers can lead to increased

Department of Electrical and Computer Engineering, University of Mohaghegh Ardabili, Ardabil, Iran. ✉email: hamid.bahador@uma.ac.ir

sensor performance[9]. Hence, this field of research is recognized as one of the key areas in nanobiotechnology and precision medicine.

Advanced nanomaterials such as graphene have attracted the attention of researchers because of their exceptional electronic and optical properties. Graphene, a single-layer carbon allotrope, exhibits exceptional electron mobility and a unique band structure, enabling the design of highly sensitive biosensors with rapid response capabilities. These features make graphene one of the main options for the development of biosensors. The use of optical plasmon properties in graphene structures, especially in the diagnosis of CEA, is considered an innovative approach[10]. This study introduces a polarization-independent LSPR sensor using a strategically engineered graphene structure with tailored cuts, achieving a sensitivity of 4.3 THz/RIU through gold nanoparticle integration, thereby overcoming the limitations of traditional LSPR sensors, such as polarization dependence and lower sensitivity, and offering significant advancements over existing designs[25,30]. The electronic properties of graphene are caused by its hexagonal grid structure, which causes the electrons to move freely. This feature increases the sensitivity of sensors and improves the signaling in the detection process[11]. In addition, graphene can absorb biological molecules to its surface, which may help increase the efficiency of sensors due to its high surface energy. graphene sensors are used not only in the identification of CEA but also in the detection of other biomarkers associated with cancer diseases[12]. In other innovative aspects, the integration of graphene with metal nanoparticles, such as gold nanoparticles, has led to an increase in the sensitivity and efficiency of sensors. This combination allows the sensors to detect very low levels of CEA, which is very important in early cancer detection[13]. Also, the development of graphene sensors with multifunctional capabilities allows for the simultaneous detection of several biomarkers, which can help doctors make therapeutic decisions[14].

Due to the strong association of CEA with different types of cancers, the development of new sensors and the optimization of existing technologies are essential for accurate and rapid measurement of this antigen. Recent research has shown that combining nanomaterials with proprietary biomolecules such as antibodies or aptamers can increase sensor performance[15]. Hence, this field of research is known as one of the key fields in nanobiotechnology and precision medicine[16].One of the new techniques in this field is the local surface plasmon deposition method LSPR, which acts based on changes in the optical properties of nanomaterials. In this method, a change in the refractive index of the environment around the nanomaterial causes a change in the intensity or wavelength of the scattered light, which is used as a sign of the presence or concentration of biomolecules. LSPR-based sensors have been highly regarded because of their high sensitivity, low sample requirements, and real-time presentation of results[17]. The benefits of this method are its high response rate and its compatibility with different types of biological molecules. However, one of the main challenges in using these sensors is the dependence on light polarization, which can affect the accuracy and repeatability of the results. To address this limitation, researchers are investigating the combination of LSPR with other materials and techniques, such as the use of high-symmetry nanomaterials or multi-polarization methods[18].

Other advances include the use of gold and silver nanoparticles in combination with LSPR sensors, which have increased the sensitivity of these sensors. Because of its strong plasmonic properties, these nanoparticles allow for the amplification of optical signals and improved detection accuracy. Such sensors can identify very small amounts of biomarkers[19]. Given the benefits and recent advances in LSPR technology, this method has become one of the key tools in the field of biosensors that can be used in the rapid and accurate diagnosis of diseases. The development of diagnostic tools and devices in the terahertz frequency range using metamaterials, such as graphene, promises significant advances in the early detection of cancer. These innovations can significantly reduce cancer-related death rates and provide patients with better treatment options[20]. the limited difference time range method (FDTD) is used to simulate and analyze the optical response of structures, focusing on its capabilities in the field of biosynthesis and optical communication[21]. Also, the CST tool is designed to calculate the absorption value of the structure and adopts the FIT integration technique for simulation.

In this article, we will examine the ultra-sensitive graphene sensor without polarization dependence to detect the CEA antigen. Using a special design of the LSPR structure, the sensor can effectively detect optical signals even in complex environments. Innovative methods in the manufacture of this sensor and its capabilities in the analysis of biological samples are considered important futurists for the development of diagnostic technologies in medicine. Finally, the results and achievements of this research can help improve early detection and monitoring of treatment for cancer patients. One of the key innovations of this paper is to provide a biosensor that can be detected faster and more reliably than traditional methods. This sensor allows for the regulation of absorption frequency based on specific clinical needs while reducing the costs and time required for diagnosis, without its accuracy being affected. The sensor responds to common problems in previous methods such as chemical and biological stability limitations and signal disturbances. These advances represent a major step towards improving diagnostic processes in medicine and can have positive effects on patients' treatment outcomes.

Simulation methodology and design

Graphene, a two-dimensional material with semi-conducting properties, plays a significant role in the field of plasmonic due to its unique characteristics. Its ability to exhibit bidirectional performance and extensive tunability makes it an attractive candidate for various applications. In summary, the integration of graphene into plasmonic structures not only enhances performance but also provides extensive opportunities for innovation across various fields, including sensing, imaging, and telecommunications[22]. Its conductivity in the terahertz range is determined by Eqs. (1) to (3). Equation (1) provides the total conductivity of graphene, obtained as the sum of intra-band and inter-band conductivity. Equation (2) calculates the inter-band conductivity and Eq. (3) allows the determination of the intra-band conductivity[23].

$$\sigma\left(\omega,\tau,\mu_c,T\right)=\sigma_{\text{inter}}\left(\omega,\tau,\mu_c,T\right)+\sigma_{\text{intera}}\left(\omega,\tau,\mu_c,T\right) \quad (1)$$

$$\sigma_{\text{inter}}(\omega,\tau,\mu_c,T) = -j\frac{e^2}{4\pi\hbar}\ln\left(\frac{2\mu_c + (\omega - j\tau^{-1})\hbar}{2\mu_c - (\omega - j\tau^{-1})\hbar}\right) \tag{2}$$

$$\sigma_{\text{intera}}(\omega,\ \tau,\ \mu_c,\ T) = -j\frac{e^2\ K_B\ T}{\pi\ \hbar^2\ (\omega\ - j\ \tau^{-1})}\left[\frac{\mu_c}{K_B\ T} + 2\ \ln\left(\exp\ \left(-\frac{\mu_c}{K_B\ T}\right) + 1\right)\right] \tag{3}$$

In the above equations, ω, angular frequency, τ, relaxation time, chemical potential of graphene, T, temperature in Kelvin (in this article, the value of $T = 300k$) e, electrical charge K_B Boltzmann's constant, ħ Planck's reduced constant are defined. According to Pauli's exclusion principle, since it is $\mu_c \gg K_B T$ in terahertz in the infrared band, the inter-band part in graphene can be ignored and the conductivity can be summarized as follows:

$$\sigma(\omega,\tau,\mu_c) = \frac{je^2\mu_c}{\pi\hbar^2(\omega + j\tau^{-1})} \tag{4}$$

Biosensor design using the proposed structure
Proposed structure with the graphene layer

According to Fig. 1 (a), which is the structure of the unit cell of the periodic system of full absorbent, Fig. 1 (b), The proposed structure has been shown to include a graphene-cut layer with a relaxation time of 2 ps, a thickness of 1 nm, the chemical potential of $\mu_c = 0.4$ eV, and temperature of 300 K. The dielectric layer, composed of silicon dioxide with a relative permittivity of 3.9[23], has a thickness of 4.2 µm and serves as an insulating substrate beneath the graphene layer. The bottom conductor layer is made of gold metal with a conductivity of 4.7×10^7[24] and a thickness of 0.3µm. The dimensions of this structure are respectively equal to W = 2.5 µm, and the radius of nine holes created in graphene is equal to r = 0.2 µm.

This structure is placed in the x and y directions as a periodic unit cell, and in the z-direction, the boundary conditions of the open space are adopted. According to the electromagnetic field theory, the absorption value A(ω) is defined as follows in Eq. (5)[25].

$$A(\omega) = 1 - R(\omega) - T(\omega) = 1 - |S_{11}(\omega)|^2 - |S_{21}(\omega)|^2 \tag{5}$$

The relation R(ω)=$|s_{11}(\omega)|^2$ shows its reflection value and T(ω)= $|s_{21}(\omega)|^2$ is the transmission amount. In the proposed structure, the copper layer prevents the passage of transmission, and T(ω)= $|s_{21}(\omega)|^2$ = 0 and the near-zero reflection coefficient is caused by the constructive interference in the resonant cavity (F-P) caused by the dielectric layer and the electric field resonance caused by the graphene layer, which causes R(ω)=$|s_{11}(\omega)|^2$ = 0, which is the value A(ω) = 1 is obtained, which indicates the highest level of absorption.

Impedance matching is a fundamental concept in the absorption of electromagnetic waves. This occurs when the impedance of a structure aligns closely with that of free space, represented as $Z_{structure} \approx Z_{air}$. Such alignment minimizes the reflection of electromagnetic waves that encounter the boundary between different materials. By adjusting parameters like the relaxation time and chemical potential of graphene, along with other factors, it is possible to modify the effective impedance of the structure, thereby achieving nearly perfect impedance matching with free space. The absorption curves of the proposed structure were drawn in Fig. 1(c) by varying the silicon dioxide thickness from 3.2 µm, 4.2 µm, and 5.2 µm. Figure 1(d) plots it with the change of gold thickness from 0.1 µm, 0.3 µm and 0.5 µm. The absorption curve shown in Fig. 1(e) is related to the refractive index of the CEA analyte with different concentrations, which is used in Table 1.

The thickness of the analyte layer affects the sensitivity and resonance shift. Figure 1(f) shows that a thickness of 1.0 µm is optimal with a sensitivity of 4.3 THz / RIU and is chosen as the basis due to the balanced plasmonic interaction, with the sensitivity stabilizing beyond 1.5 µm.

To study the behavior of the sensor, the refractive index corresponding to various concentrations of carcinoembryonic antigen (CEA) has been considered. Subsequently, the sensor structure is simulated under similar conditions. As a result, the sensitivity of the sensor can be calculated based on the frequency shift of resonance in response to changes in the refractive index[26].

$$\text{S} = \frac{\Delta f}{\Delta n} \tag{6}$$

Moreover, FOM is defined as[26]:

$$\text{FOM} = \frac{\text{S}}{\text{FWHM}} \tag{7}$$

where FWHM denotes the full width at half maximum, this characteristic, alongside the quality factor (Q), defined as Q = f/FWHM, is used to evaluate the sensor's performance. Based on Table 2, five samples of carcinoembryonic antigen (CEA) concentrations with refractive indices ranging from 1.3337 to 1.3485 are placed in the analyte layer. These samples are then simulated, and their absorption spectra are plotted and illustrated in Fig. 1 (e).

A closer examination of Table 2, derived from the absorption curve shown in Fig. 1 (e), reveals that the absorption value at all analyte concentrations exceeds 99%, indicating complete absorption. This measurement has a FWHM of approximately 210 GHz. The average quality factor is approximately 40, with a maximum sensitivity of 1.98 THz/RIU. The figure of merit (FOM) was calculated using the formula provided in the study,

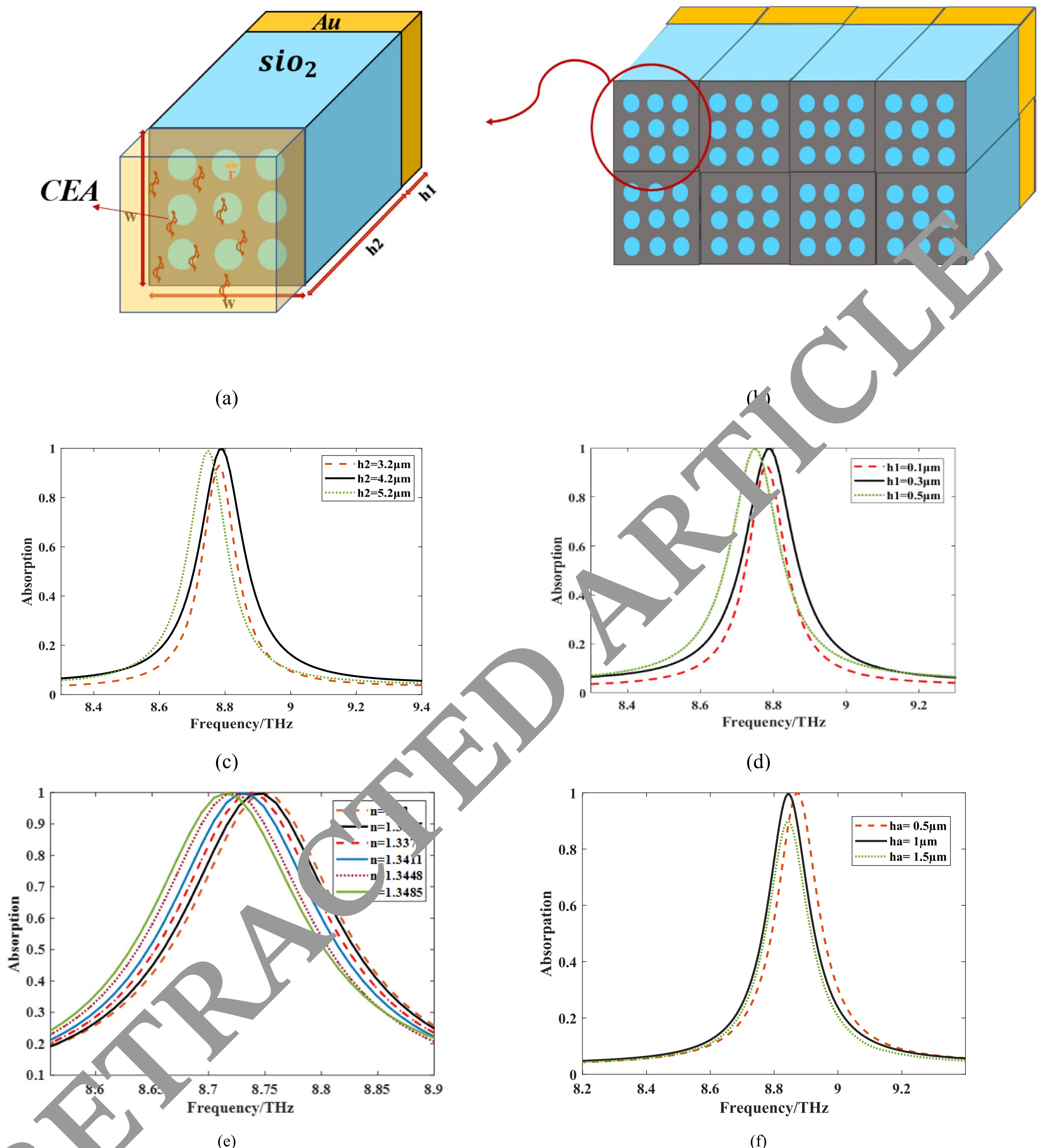

Fig. 1. (**a**) A cell of the periodic structure (**b**) Complete structure of a complete absorber (**c**) varying the silicon dioxide thickness from 3.2 µm, 4.2 µm, and 5.2 µm. (**d**) Absorption curve of the gold thickness from 0.1 µm, 0.3 µm, and 0.5 µm (e) related to the refractive index of the CEA analyte with different concentrations (**f**) Absorption spectrum of analyte with different thickness.

and the limit of detection (LOD), which denotes the minimum detectable quantity of an analyte in a sample, is calculated using the formula $\text{LOD} = F_r / (20_* S_* Q)$[27]. We will incorporate gold nanoparticles in the subsequent section to enhance these results.

Proposed structure with graphene layer and gold nanoparticles

The frequency-absorbing structure designed for use in a biosensor based on graphene and gold nanoparticles represents an innovative approach to enhancing sensitivity and selectivity in the detection of biomolecules.

CEA concentration (ng/ml(	$n = n_0 + \Delta n$
1	1.3337
2	1.3374
3	1.3411
4	1.3448
5	1.3485

Table 1. The corresponding refractive index of CEA concentrations **(n_0 = 1.33)**[26].

Refractive index	Freq (THz)	Abs. (%)	FWHM (THz)	Q-Factor	Sensitivity (THz/RIU)	FOM	LOD
n = 1.33	8.749053	99.9	0.217	40.13	—	—	—
n = 1.3337	8.743953	99.4	0.212	41	1.38	6.35	[illegible]
n = 1.3374	8.738037	99.9	0.21	40.1	1.49	[illegible]	0.0073
n = 1.3411	8.727064	99.7	0.208	40.6	1.98	[illegible]	0.0055
n = 1.3448	8.721063	99.5	0.214	41.1	1.89	[illegible]	[illegible]
n = 1.3485	8.716024	99.9	0.216	41.3	1.79	8.23	0.0061

Table 2. The results derived from the variations in the refractive index of the analyte layer corresponding to different concentrations of carcinoembryonic antigen (CEA) are presented.

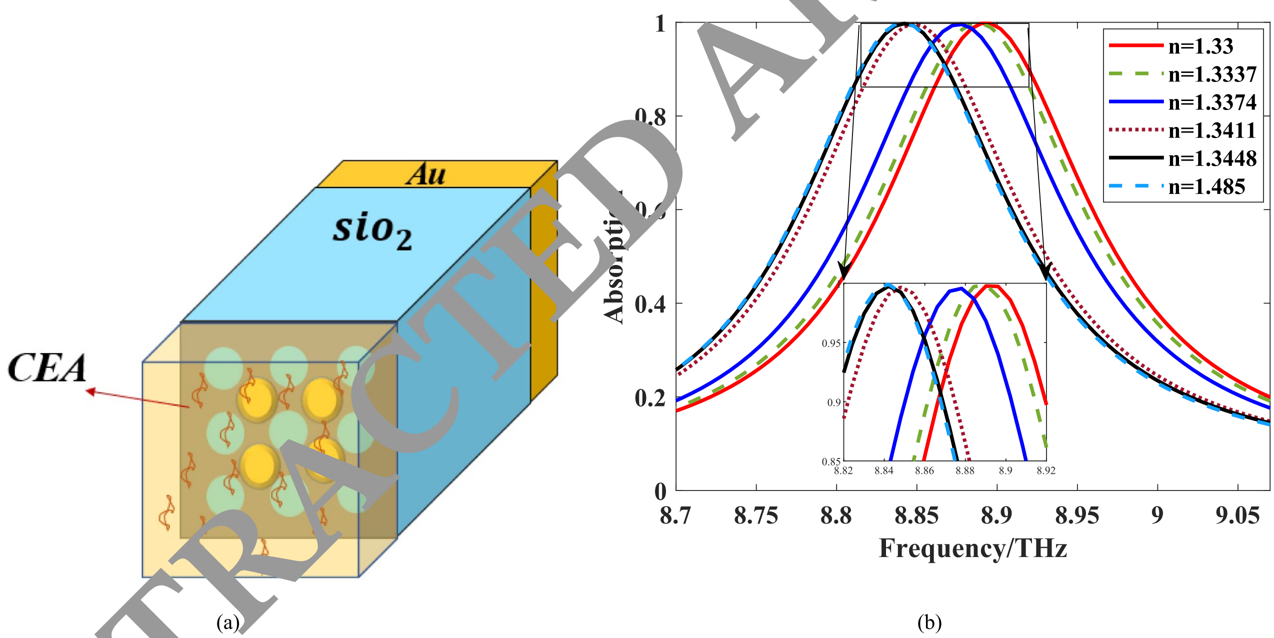

Fig. 2. (**a**) A cell of the periodic structure (**b**) related to the refractive index of the CEA analyte with different concentrations.

the graphene layer is the sensitive component, providing improved interaction with target molecules due to its tunable electronic properties and high surface-to-volume ratio. gold nanoparticles, which can be dispersed or patterned on the graphene, enhance local electromagnetic fields through plasmonic effects, creating suitable binding sites for biomolecules. this design offers high sensitivity due to the amplification of electromagnetic fields and supports use in compact and multifunctional devices, thanks to the tunable properties of graphene and its compact design.

According to Fig. 2(a), with the placement of gold nanowires with a radius of 0.2 µm and a thickness of 0.1 µm, all sizes of graphene, silicon dioxide, and gold substrate are the same as the structure of Fig. 1(a), and the only difference is the placement of gold nanoparticles. Suppose that the absorption curve of graphene structure along with gold nanowires for different concentrations of CEA analyte is shown in Fig. 2(b).

Table 3 from the analysis of Fig. 2 (b), which is the curve of the proposed structure of the graphene layer with gold nanoparticles, by comparing Table 2 and Table 3, we can make some basic points about the absorbents according to the output of the measured values, which received a frequency.

Refractive index	Freq (THz)	Abs. (%)	FWHM (THz)	Q-Factor	Sensitivity (THz/RIU)	FOM	LOD
n = 1.33	8.8961	99.7	0.163	54.6	—	—	—
n = 1.3337	8.8875	99.9	0.163	54.5	2.324	14.26	0.0035
n = 1.3374	8.8763	99.6	0.163	54.5	2.675	16.43	0.003
n = 1.3411	8.8483	99.7	0.164	53.9	4.306	26.24	0.0019
n = 1.3448	8.8433	99.8	0.164	54	3.567	21.79	0.0022
n = 1.3485	8.8402	100	0.164	53.8	3.022	18.41	0.0027

Table 3. The results derived from the variations in the refractive index of the analyte layer corresponding to different concentrations of carcinoembryonic antigen (CEA) are presented.

Design	Year	Operating Frequency Band (THz)	Sensitivity	FOM	Q-Factor (RIU^{-1})	Analyte
Four Trishul structures with a cross-aperture in the center[30]	2021	6.0—7.0	0.196 THz/RIU	19.65	165	Refractive Index
Two-layer graphene disk[30]	2020	7.0—8.0	1.1 THz/RIU	12.5	25.8	Breast Cancer
Graphene semicircle rings[31]	2022	7.5—8.5	1.4 THz/RIU	17.3	40.52	Refractive Index
Five-segment[26]	2019	8.0—9.0	1.44 THz/RIU	26.6	[illegible]	CEA
Cu/CNT/$HfSe_2$/Prism[29]	2023	5.0—6.0	350 deg/RIU	---	---	Colorectal cancer
$PtSe_2$/Graphene SPR sensor[32]	2021	6.5—7.5	235 deg/RIU	[illegible]	---	Breast type II cancer, skin cancer
WTe_2/Ag SPR gas sensor[33]	2022	5.5—6.5	374.31 deg/RIU	[illegible]	---	NO_2, flammable/toxic gases
LRSPR Gr/Cu biosensor[34]	2023	7.0—8.0	4655.7 RIU	[illegible]	---	E. coli, pathogens
Au–Ag/WS_2 SPR sensor[35]	2020	6.0—7.0	304 deg/RIU	[illegible]	---	Skin, cervical, breast cancers
ZnO–Si–Ag SPR sensor[36]	2021	5.5—6.5	311 deg/RIU	[illegible]	---	Acetone, D_2O (RI = 1.33–1.36)
Bimetallic–MXene–Graphene SPR[37]	2022	6.5—7.5	301.17 deg/RIU		---	Malaria biomarkers
This work ONLY GRAPHENE LAYER	2025	8.4—9.2	1.98 THz/RIU	9.13	40.6	CEA
This work GRAPHENE LAYER AND GOLD NANOPARTICLES	2025	8.4—9.2	4.3 THz/RIU	26.2	54.5	CEA

Table 4. Comparing the results of the proposed structure with the results of previous works.

First, the sensitivity values of the two proposed structures are compared. The addition of gold nanoparticles significantly increases the sensitivity, reaching up to three times the value of the structure without gold for certain analyte refractive indices. However, despite this advantage, the linearity of sensitivity in the first structure, which contained only a graphene layer, has decreased. This suggests a trade-off between high sensitivity and reduced linearity in sensitivity values when gold nanoparticles are added.

In the next stage of the comparison, the value of FWHM has been reduced with the decoration of gold nanoparticles, which is a positive point for the second structure. The value of the quality factor and FOM has also increased in the second structure, and the LOD value in the second structure is significantly lower. This can be considered one of the important advantages of the second structure with gold nanoparticles. Similarly, heterostructure-based refractive index sensors combining 2D materials such as $PtSe_2$ and graphene have shown promising results in cancer diagnostics, especially for breast and skin cancers[28]. These findings support the continued integration of multiple nanomaterials to enhance optical sensing performance. Similar to recent multilayer designs targeting colorectal cancer diagnosis with refractive index sensitivities exceeding 350 deg/RIU in the range of 1.33–1.35[29], our proposed graphene-gold nanoparticle-based structure also demonstrates superior sensitivity (4.3 THz/RIU) and figure of merit (26.2), making it a competitive alternative in the terahertz range.

Table 4 compares the proposed structure in this study with previous works in terms of design, sensitivity, FoM, Q-Factor, and analyte. The proposed structure demonstrates significantly higher sensitivity (4.3 THz/RIU) and FoM (26.2) compared to earlier designs, such as the "four Trishul structure" (0.196 THz/RIU) and "two-layer graphene disk" (1.1 THz/RIU). Additionally, the Q-Factor of the proposed design (54.5) outperforms other designs, highlighting its superior capability in analyte detection. While prior studies targeted analytes like refractive index and breast cancer biomarkers, this study focuses on CEA detection, achieving enhanced precision. These results emphasize the effectiveness of the proposed design for bio-sensing applications, surpassing the limitations of previous works. Recent theoretical studies have demonstrated that integrating 2D materials such as WTe_2 with traditional SPR structures can significantly enhance the detection of organic materials, achieving sensitivities up to 213.75 deg/RIU in the Kretschmann configuration[33]. These findings support the continued exploration of 2D material-based hybrid platforms for achieving superior sensing performance, as reflected in our graphene-gold nanoparticle terahertz absorber. 2S2G/Cytop/Cu/Graphene configuration, have reported exceptional imaging sensitivity (up to 4655.7 RIU^{-1}) and figure of merit values (up to 781.5 RIU^{-1}), particularly in detecting bacterial pathogens[34]. These findings align with our results in enhancing FOM and sensitivity via graphene-gold hybrid structures for terahertz-based biosensing. Dichalcogenides like WS_2 have achieved high sensitivity (up to 304°/RIU) and FoM values of ~ 39, particularly for cancer detection applications[35]. Our proposed structure achieves comparable performance in the THz domain using graphene-gold nanoparticle configurations, further validating the effectiveness of a 2D material hybrid. Recent studies employing multilayer black phosphorus in combination with noble metals for gas sensing have reported high performance parameters, such as a sensitivity of 374.31°/RIU and FoM of 37.63, emphasizing the impact of 2D material integration in enhancing SPR sensor designs[36]. Our proposed graphene-gold nanoparticle hybrid achieves similar levels of enhancement in terahertz-based biosensing. SPR sensors incorporating ZnO-Si-Ag multilayers have shown high sensitivity (up to 311°/RIU) and figure of merit values exceeding 70/RIU in detecting analytes with RI ranging from 1.3264 to 1.36[37]. These findings further emphasize the benefits of multilayer nanostructure designs for improving optical biosensing, consistent with our graphene-gold absorber sensor's high THz sensitivity and FOM. The incorporation of 2D materials such as MXene and graphene in bimetallic SPR biosensors has recently achieved sensitivity values exceeding 301°/RIU for malaria detection, underscoring the growing utility of layered nanostructures for biomedical diagnostics. Our proposed graphene-gold THz sensor shows similar advancements for cancer biomarker CEA detection, with improved FOM and LOD performance.

Independent of polarization

Figure 3 (a) shows that the resonance peak value remains consistent despite varying the polarization angle between 0°, 120°, and 270°. This indicates that the shape of the diagram remains unchanged across these three polarization angles, suggesting that the biosensor structure is polarization-independent. This characteristic is beneficial as it enhances the practicality and suitability of the biosensor for detecting specific analytes. So, the biosensor's performance remains stable and reliable regardless of the polarization angle used, which is advantageous for its application in analytical tasks such as detecting desired analytes. Figure 3(b) illustrates a magnetic wave with oblique radiation that influences both the absorption characteristics and the angular stability capability. These features are analyzed across a range of angles, depending on the value of θ, at which the absorber exhibits nearly constant characteristics. Consequently, the proposed terahertz absorber demonstrates remarkable stability against variations in the angle of incidence from 0 to 60 degrees. Given the inherent polarization of the terahertz absorber, its behavior remains non-sensitive and similar for both TM (Transverse Magnetic) and TE (Transverse Electric) modes of propagation. Therefore, it can be concluded that the proposed absorber maintains high stability against changes in the incoming radiation's angle and intensity.

Analysis and design of equivalent circuit for frequency absorber

This section focuses on the analysis and design of an equivalent circuit for a frequency absorber. Initially, the overall structure of the equivalent circuit and its components are introduced. Following this, the frequency absorption graph of the circuit is presented, illustrating its performance within the desired frequency range. Subsequently, the mathematical equations relevant to calculating input impedance, wave propagation coefficient, and other important parameters of the circuit are provided. These equations enable precise calculation of resistance, inductance, and capacitance values within the structure. The goal of this analysis is to optimize the performance of the frequency absorber by utilizing the unique properties of graphene layers.

The equivalent circuit with lumped elements for the absorber is designed and shown in Fig. 4(a). The substrate is modeled with a short circuit with impedance zero, which in this proposed structure is made of copper. A connecting line with impedance Z_{TL} and electrical length $E_{TL} = 2 \times \beta_{TL} \times T_S$ is used to model SiO_2. Each graphene layer can be modeled as a combination of resistive (R), and capacitive (C), inductive (L) components in parallel. The total input impedance (Z_{in}) of the network can be found by combining the impedances of all

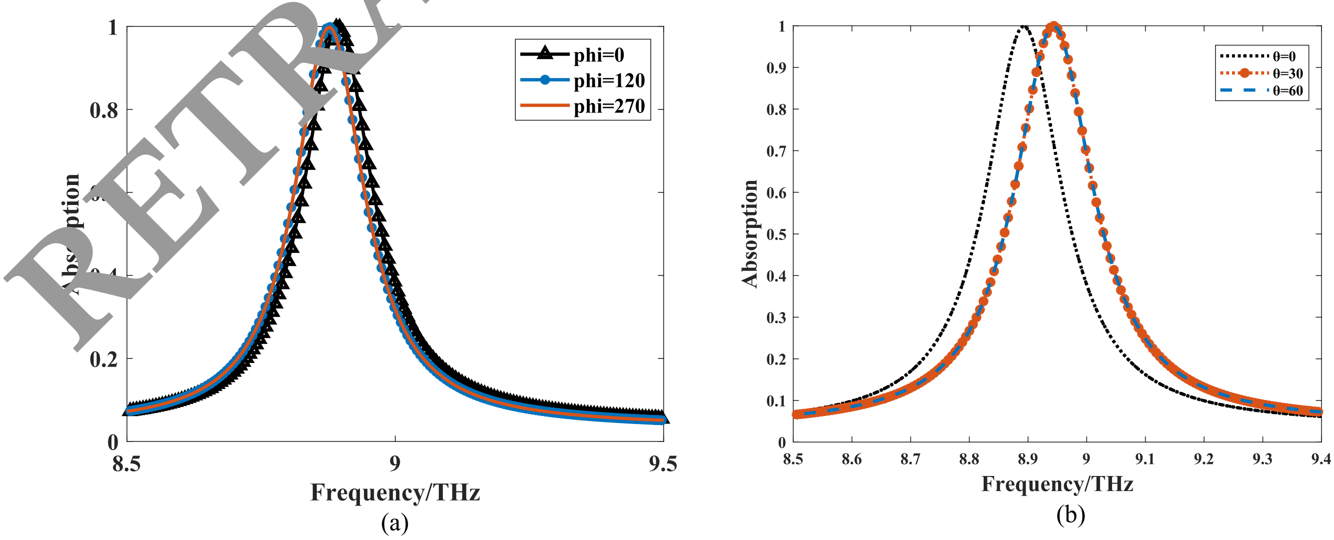

Fig. 3. (**a**) Absorption curve with three different polarization angles. (**b**) output frequency spectrum for different values of radiation angle.

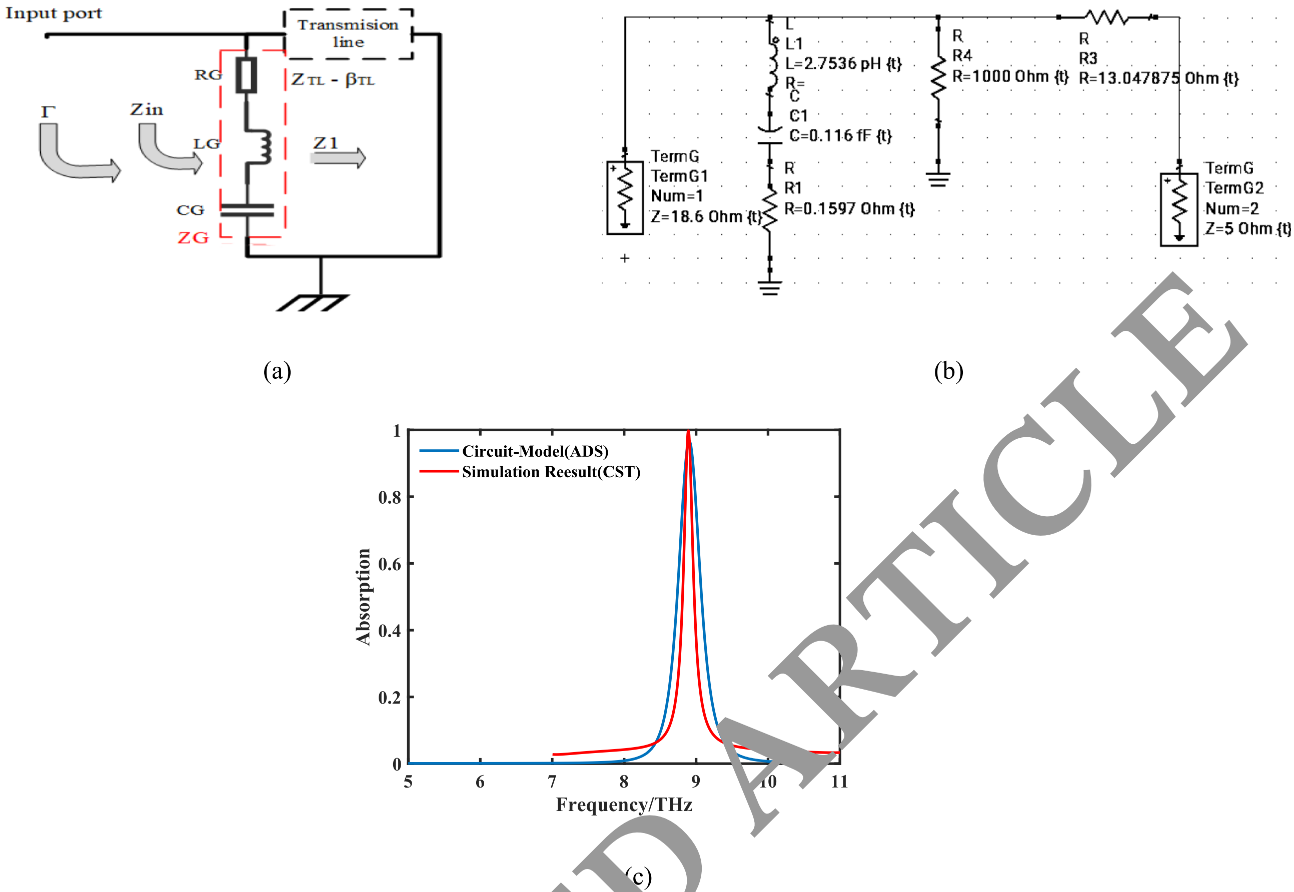

Fig. 4. (**a**) The general scheme of the equivalent circuit of the frequency absorber (**b**) the equivalent circuit of the absorber structure is designed by ADS (**c**) the absorption curve of the circuit model and simulation.

branches. The free space impedance is given as 377 Ω (or 120π Ω). When calculating the input impedance relative to free space, you might consider matching conditions that can affect R, L, and C values to optimize performance[38]:

$$Z_1 = jZ_{TL}\tan(\beta_{TL}T_s) \tag{8}$$

$$\beta_{TL} = 2\pi f\sqrt{\varepsilon_0\varepsilon_r\mu_0} \tag{9}$$

$$Z_{TL} = \sqrt{\mu_0/\varepsilon_0\varepsilon_r} \tag{10}$$

$$Z_G(f) = R + jX_G = R + j(2\pi fL - \frac{1}{2\pi fC}) = \frac{1}{\sigma_g(f)} \tag{11}$$

$$Z_{in} = \frac{Z_1.Z_g}{Z_1 + Z_g} \tag{12}$$

where β_{TL} and ε_r represent the wave number and relative permittivity of the dielectric, respectively. Additionally, the following equations can be utilized to calculate the values of resistance (R), inductance (L), and capacitance (C) in a structure consisting of graphene layers. These equations are related to various factors, including the magnetic permeability (μ_r) and the relative permittivity (ε_r)[39]:

$$R = \frac{KL^2}{\pi S^2}\frac{\hbar^2}{e^3\mu_c\tau} \quad , L = \frac{KL^2}{\pi S^2}\frac{\hbar^2}{e^3\mu_c} \quad , C = \frac{\pi^2 S^2}{L^2 k}\frac{\varepsilon}{q_1}$$

Figure 4(b) shows the equivalent circuit of the absorber structure designed by ADS software. Part of the simulations in this work was performed using Keysight Advanced Design System (ADS), version 2024[40]. Also, the absorption curve of the circuit model (ADS) and simulation (CST) is shown in Fig. 4(c).

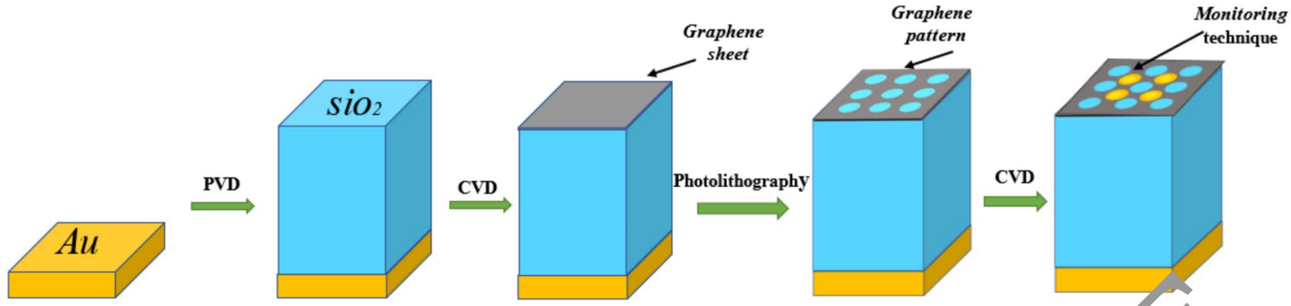

Fig. 5. The fabrication procedure for the proposed metamaterial absorber.

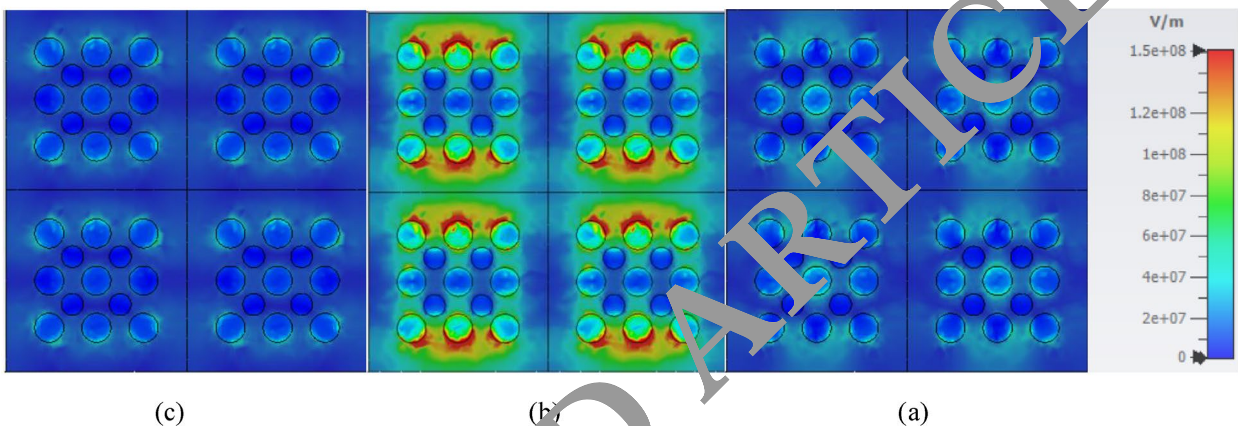

Fig. 6. Electric field [real (Ez)] distribution in the normal incidence of TE waves at frequencies of (**a**) 8 THz, (**b**) 8.89 THz, (**c**)10 THz.

Fabrication process of the gold graphene structure with nanoparticles

The conductive layer, composed of gold for this simulation, is located at the bottom of the structure. Following this, a dielectric layer made of silicon oxide is deposited on top of the gold layer using the physical vapor deposition (PVD) technique. Subsequently, a graphene layer is applied onto the silicon oxide via the chemical vapor deposition (CVD) method. Photolithography is then employed to etch patterns into the graphene, achieving the desired structural design. In the next step, gold nanoparticles are deposited onto the graphene layer using the CVD technique, with their thickness carefully controlled through a monitoring technique. This entire fabrication process results in the overall structure illustrated in Fig. 5.

Chemical vapor deposition (CVD) enables the fabrication of nanostructured metamaterials, including graphene-based designs, tailored for specific terahertz absorption characteristics. These structures, especially when combined with graphene, can have very interesting applications in material identification and biorecognition. With a standard lithography process, graphene can be fabricated and placed into special structures that can provide favorable THz responses to aqueous environments and biomolecules. Finally, measuring absorption values using THz time-domain spectroscopic systems allows researchers to obtain detailed information about the material content, its changes under different conditions, and the possible effects of biological particles on optical properties. This type of analysis can help better understand materials' behavior in the terahertz region and lead to the development of new technologies and applications[41].

It is important to emphasize that the following fabrication steps are presented as a theoretical and conceptual guideline based on standard fabrication techniques commonly reported in the literature. These steps were not performed experimentally in this study. Instead, they are included to demonstrate the potential feasibility of implementing the proposed simulated structure in practical fabrication scenarios, and to support future experimental endeavors.

Figure 6 illustrates the scattering of the electric field [real (Ez)] in the TE mode, examined across different frequencies. As depicted in Fig. 6(a), at a frequency of 8 terahertz, the field distribution shows lower density at the upper and lower edges due to its distance from the resonance peak frequency. Additionally, Fig. 6(b) presents the field distribution at a frequency of 8.89 terahertz, where the field exhibits a horizontal configuration, with increased density at the upper and lower edges. Finally, Fig. 6(c) displays the field distribution at a frequency of 10 terahertz, which again shows lower density at the upper and lower edges due to its distance from the resonance peak frequency. These results demonstrate significant variations in the electric field distribution as the frequency changes.

Conclusion

In summary, this research presents the design and evaluation of an optimized biosensor with high absorption efficiency near the frequency of 8.89 THz. The first structure achieved absorption rates ranging from 99.4% to 99.9%, while the second structure, which incorporates both graphene and gold nanoparticles, reached absorption rates between 99.6% and 100%. Contains graphene plus gold nanoparticles. These high absorption rates make the sensor an excellent candidate for biosensing applications, especially for the detection of CEA in clinical samples. By testing the sensor with analytes containing CEA in concentrations of 1, 2, 3, 4, and 5 ng/ml, the refractive index values were 1.3337, 1.33374, 1.3448, and 1.3485, respectively. When the analyte layer is placed on the adsorbent structure, the absorption peak shifts, which allows the detection of the analyte of interest. The proposed structure showed significant sensitivity and achieved 4.3 THz / RIU at a refractive index of 1.3411 and a frequency of 8.8483 THz.in general, this biosensor has wide applications in the fields of medicine, environment, biosecurity, and industry, and it can create a revolution in disease diagnosis methods.

Data availability

The data that support the findings of this study are available from the corresponding author upon reasonable request.

Received: 7 March 2025; Accepted: 21 August 2025
Published online: 26 August 2025

References

1. Das, S., Saha, B., Tiwari, M. & Tiwari, D. K. Diagnosis of cancer using carbon nanomaterial-based biosensors. *Sens. Diagn.* **2**(2), 268–289 (2023).
2. Hasan, M. R. et al. Recent development in electrochemical biosensors for cancer biomarkers detection. *Biosens. Bioelectron. X* **8**, 100075 (2021).
3. Hall, C. et al. A review of the role of carcinoembryonic antigen in clinical practice. *Ann. Coloproctol.* **35**(6), 294 (2019).
4. Goldenberg, D. M. et al. CEA (carcinoembryonic antigen): Its role as a marker in the management of cancer. *J. Cancer Res. Clin. Oncol.* **101**(3), 239–242. https://doi.org/10.1007/BF00410[illegible] (1981).
5. Shahazi, R. et al. Recent progress in Nanomaterial based biosensors for the detection of cancer biomarkers in human fluids. *Nano Carbons* **2**(2), 1254–1254 (2024).
6. Iftikhar, F. J., Shah, A., Wali, Q. & Kokab, T. Advancements in nanofiber-based electrochemical biosensors for diagnostic applications. *Biosensors* **13**(4), 416 (2023).
7. Aghaei, F., Golmohammadi, S., Bahador, H. & Soofi, H. Design of a high-sensitivity graphene-silicon hybrid micro-disk in a square cavity whispering gallery mode biosensor. *J Nanopart Res* **25**(4), 76. https://doi.org/10.1007/s11051-023-05724-3 (2023).
8. Zhang, L. et al. Recent advances in nanomaterial-based biosensors for the detection of exosomes. *Anal. Bioanal. Chem.* **413**(1), 83–102. https://doi.org/10.1007/s00216-020-0[illegible] (2021).
9. Li, X., Ma, F., Yang, M. & Zhang, J. Nanomaterial based analytical methods for breast cancer biomarker detection. *Mater. Today Adv.* **14**, 100219 (2022).
10. Wei, S., Chen, X., Zhang, X. & Chen, [illegible] Recent development of graphene based electrochemical sensor for detecting hematological malignancies-associated biomarkers: A mini-review. *Front. Chem.* **9**, 735668 (2021).
11. Bai, Y., Xu, T. & Zhang, X. Graphene-based biosensors for detection of biomarkers. *Micromachines* **11**(1), 60 (2020).
12. Lin, L. P. & Tan, M. T. T. Biosensors for the detection of lung cancer biomarkers: A review on biomarkers, transducing techniques and recent graphene-based implementations. *Biosens. Bioelectron.* **237**, 115492 (2023).
13. Mostufa, S., Akib, T. B. A., Rana, M. M. & Islam, M. R. Highly sensitive TiO2/Au/graphene layer-based surface plasmon resonance biosensor for cancer detection. *Biosensors* **12**(8), 603 (2022).
14. Hosseini, S. M. et al. Multifunctional Carbon-Based Nanoparticles: Theranostic Applications in Cancer Therapy and Diagnosis. *ACS Appl. Bio Mater.* **6**(4), 1323–1338. https://doi.org/10.1021/acsabm.2c01000 (2023).
15. Hu, Y. et al. Recent advances in nanomaterials for prostate cancer detection and diagnosis. *J. Mater. Chem. B* **10**(26), 4907–4934 (2022).
16. Chaudhary, V., Vasistha, S. & Rai, M. P. Nanobiotechnology: an Applicable Approach for Sustainable Future. In *Emerging Sustainable Nanomaterials for Biomedical Applications* (eds Garg, S. et al.) 243–268 (Springer Nature, 2024).
17. [illegible] et al. Bioelectronic modulation of single-wavelength localized surface plasmon resonance (LSPR) for the detection of electroactive biomolecules. *Chin. Chem. Lett.* **33**(6), 3144–3150 (2022).
18. Mayer, K. M. & Hafner, J. H. Localized Surface Plasmon Resonance Sensors. *Chem. Rev.* **111**(6), 3828–3857. https://doi.org/10.1021/cr100313v (2011).
19. Anker, J. N. et al. Biosensing with plasmonic nanosensors. *Nat. Mater.* **7**(6), 442–453 (2008).
20. Khan, S. A. et al. Optical Sensing by Metamaterials and Metasurfaces: From Physics to Biomolecule Detection. *Adv. Opt. Mater.* **10**(18), 2200500. https://doi.org/10.1002/adom.202200500 (2022).
21. Masoudian Saadabad, R., Huang, L., Evlyukhin, A. B. & Miroshnichenko, A. E. Multifaceted anapole: From physics to applications. *Opt. Mater. Expr.* **12**(5), 1817–1837 (2022).
22. Farmani, A., Mir, A. & Sharifpour, Z. Broadly tunable and bidirectional terahertz graphene plasmonic switch based on enhanced Goos-Hänchen effect. *Appl. Surf. Sci.* **453**, 358–364 (2018).
23. Y. Rafighirani, J. Javidan, and H. Heidarzadeh, "Development of a Multi-Band High-Sensitivity Polarization-Independent Absorber: A Biosensor for Simultaneous Detection of Multiple Cancer Biomarkers," *Plasmonics*, pp. 1–9, (2024).
24. Pilehroudi, A., Javidan, J., Rafighirani, Y. & Heidarzadeh, H. Three-Band Graphene-Based Fully Independent Polarization Absorber for Biosensing Applications. *Plasmonics* https://doi.org/10.1007/s11468-024-02614-9 (2024).
25. Errajraji, K. et al. Design and analysis of a multi-band miniaturized metamaterial absorber for wireless communication applications. *Opt. Quant Electr.* **56**(2), 232. https://doi.org/10.1007/s11082-023-05813-6 (2024).
26. H. Bahador, "Five-segment THz refractive index metamaterial biosensor with perfect absorption for carcinoembryonic antigen measurement," *IEEE Sensors Journal*, (Accessed 02 Jan 2025). [Online]. https://ieeexplore.ieee.org/abstract/document/10597354/. (2024).
27. Khodaie, A. & Heidarzadeh, H. Split Ring Resonator-Based Multimode Plasmonic Optical Biosensors for Comprehensive Antigen Detection. *Sens Imag.* **25**(1), 63. https://doi.org/10.1007/s11220-024-00514-0 (2024).
28. Karki, B., Sarkar, P., Dhiman, G., Srivastava, G. & Kumar, M. Platinum Diselenide and Graphene-Based Refractive Index Sensor for Cancer Detection. *Plasmonics* **19**(2), 953–962. https://doi.org/10.1007/s11468-023-02051-0 (2024).
29. Karki, B., Pal, A., Dhiman, G. & Ahmed, M. Z. Ultra-sensitive early detection of colorectal cancer using surface plasmon resonance sensor: Theoretical analysis. *Microchim. Acta* **192**(2), 126. https://doi.org/10.1007/s00604-025-06983-8 (2025).

30. Manikandan, E., Karthigeyan, K. A., Arivarasi, A. & Papanasam, E. High-Q and FOM dual-band polarization dependent ultra-narrowband terahertz metamaterial sensor. *IEEE Photonics J.* **15**(1), 1–6 (2023).
31. Liang, D. & Chen, T. Optical modulated graphene metamaterial based on plasmon-induced transparency in the terahertz band: Application for sensing. *Diam. Relat. Mater.* **131**, 109613 (2023).
32. Karki, B., Uniyal, A., Sharma, M., Yadav, R. B. & Buduma, P. Tuning sensitivity of bimetallic, MXene and graphene-based SPR biosensors for rapid malaria detection: a numerical approach. *J. Comput. Electron.* **23**(4), 920–929. https://doi.org/10.1007/s10825-024-02191-4 (2024).
33. Karki, B., Sarkar, P., Mahmoud, K. H., Alsubaie, A. S. & Sharma, M. Detection of Organic Material Using Tungsten Ditelluride Based Surface Plasmon Resonance Sensor. *Plasmonics* https://doi.org/10.1007/s11468-024-02356-8 (2024).
34. Karki, B., Pal, A., Alsubaie, A. S., Mahmoud, K. H. & Sharma, M. Detection of pathogens in water using long range surface plasmon resonance biosensor: numerical investigation. *Physica B* **695**, 416503 (2024).
35. Karki, B., Alsubaie, A. S., Sarkar, P., Sharma, M. & Ali, N. B. Detection of Skin, Cervical, and Breast Cancer Using Au–Ag Alloy and WS2-Based Surface Plasmon Resonance Sensor. *Plasmonics* https://doi.org/10.1007/s11468-024-02521-z (2024).
36. Karki, B., Trabelsi, Y., Sarkar, P., Pal, A. & Uniyal, A. Tuning sensitivity of surface plasmon resonance gas sensor based on multilayer black phosphorous. *Mod. Phys. Lett. B* **39**(01), 2450364. https://doi.org/10.1142/S0217984924503640 (2025).
37. Karki, B. et al. ZnO-Silicon Enhanced Surface Plasmon Resonance Sensor for Chemical Sensing. *SILICON* [illegible], [illegible]–3872. https://doi.org/10.1007/s12633-024-02973-2 (2024).
38. Norouzi-Razani, A. & Rezaei, P. Multiband polarization insensitive and tunable terahertz metamaterial perfect absorber based on the heterogeneous structure of graphene. *Opt. Quant Electr.* **54**(7), 407. https://doi.org/10.1007/s11082-022-0381[illegible]6 (2022).
39. Rezagholizadeh, E., Biabanifard, M. & Borzooei, S. Analytical design of tunable THz refractive index sensor for TE and TM modes using graphene disks. *J. Phys. D Appl. Phys.* **53**(29), 295107 (2020).
40. "Advanced Design System (ADS) | Keysight." Accessed 11 Aug. 2025. [Online]. https://www.keysight.com/zz/en/products/software/pathwave-design-software/pathwave-advanced-design-system.html
41. Rafighirani, Y., Javidan, J. & Heidarzadeh, H. Polarization-independent tunable multi-band terahertz absorber based on graphene structure to design the ultra-high sensitive biosensors. *Phys. Scr.* **99**(7), 075014 (2024).

Author contributions

Y.R. : Methodology, Software, Investigation, Resources, Writing – original draft. H.B. : Validation, Conceptualization, Writing – review & editing, Supervision. J.J. : Validation, Conceptualization and Writing.

Declarations

Competing interests

The authors declare no competing interests.

Additional information

Correspondence and requests for materials should be addressed to H.B.